SAMHD1 enhances immunoglobulin hypermutation by promoting transversion mutation

Eddy Sanchai Thientosapol[a,b], Daniel Bosnjak[a,b], Timothy Durack[a,b], Igor Stevanovski[a,b], Michelle van Geldermalsen[a,b], Jeff Holst[a,b], Zeenat Jahan[a,b], Caitlin Shepard[c], Wolfgang Weninger[a,b], Baek Kim[c,d], Robert Brink[e], and Christopher J. Jolly[a,b,1]

[a]Centenary Institute, Camperdown NSW 2050, Australia; [b]Sydney Medical School, The University of Sydney, Sydney, NSW 2006, Australia; [c]Emory School of Medicine, Emory University, Atlanta, GA 30322; [d]School of Pharmacy, Kyung Hee University, 02447 Seoul, South Korea; and [e]Garvan Institute of Medical Research, Darlinghurst, Sydney, NSW 2010, Australia

Edited by David G. Schatz, Howard Hughes Medical Institute and Yale University School of Medicine, New Haven, CT, and accepted by Editorial Board Member Robert L. Coffman March 28, 2018 (received for review November 15, 2017)

Activation-induced deaminase (AID) initiates hypermutation of *Ig* genes in activated B cells by converting C:G into U:G base pairs. G_1-phase variants of uracil base excision repair (BER) and mismatch repair (MMR) then deploy translesion polymerases including REV1 and Pol η, which exacerbates mutation. dNTP paucity may contribute to hypermutation, because dNTP levels are reduced in G_1 phase to inhibit viral replication. To derestrict G_1-phase dNTP supply, we CRISPR-inactivated SAMHD1 (which degrades dNTPs) in germinal center B cells. *Samhd1* inactivation increased B cell virus susceptibility, increased transition mutations at C:G base pairs, and substantially decreased transversion mutations at A:T and C:G base pairs in both strands. We conclude that SAMHD1's restriction of dNTP supply enhances AID's mutagenicity and that the evolution of *Ig* hypermutation included the repurposing of antiviral mechanisms based on dNTP starvation.

B cells | mutation | DNA repair | dNTPs | deamination

Somatic hypermutation, in combination with clonal selection, creates high-affinity antibodies (Ig) in response to viral and bacterial infection. Activation-induced deaminase (AID, gene *Aicda*) initiates mutation by deaminating genomic cytosines, in either strand of *Ig* V(D)J-regions, which creates a U:G mismatch in the DNA (Fig. S1). If replication proceeds without uracil excision, this produces a C:G to T:A transition mutation in one daughter cell, because A is incorporated opposite U (reviewed in ref. 1).

Most deaminations are excised by the base excision repair (BER) enzyme UNG2, a uracil-specific enzyme that converts U into an apyrimidinic (AP) site (Fig. S1). The enzymes SMUG1 and TDG can substitute for UNG2, but in UNG2-proficient cells, their contribution to *Ig* hypermutation is probably minor (2–5). Mismatch repair (MMR) is also recruited (Fig. S1), presumably by the U:G mismatches deamination induces. Processing via BER or MMR predominantly restores C in place of U (6–9) but is also error-prone. Error-prone BER converts deamination sites into transition or transversion mutations at C/G and occasionally produces mutations at bases flanking deamination sites, including A/T bases (1). Mutation does not require the canonical BER polymerase, Pol β (10); instead, C/G to G/C transversion mutation requires the translesion polymerases REV1 and Pol η (11, 12). Bypass of persistent AP sites using translesion polymerases is therefore thought to be the main mechanism of UNG2-dependent *Ig* hypermutation (12, 13).

Mutation at *Ig* A:T base pairs is substantially reduced by inactivation of the MMR genes *Msh2, Msh6*, or *Exo1,* inactivation of *Polh*, or by mutation of the K164 ubiquitination site in mouse PCNA (14–19). This has led to a model in which A/T mutations are introduced by translesion Pol η, predominantly recruited by noncanonical MMR (1, 20), with minor recruitment during UNG2-driven long patch (LP) BER (21). In this model (Fig. S1), activated MutSα recruits ExoI to create excision patches. Monoubiquitinated PCNA then recruits error-prone Pol η during excision patch in-fill, which introduces mutations biased toward A:T base pairs. Until recently, it was unknown how the DNA was nicked to allow ExoI entry, but it is now clear that APE1, APE2, and MutLα produce nicks semiredundantly (4, 5, 22) (Fig. S1).

A major question raised by this model is why PCNA becomes ubiquitinated to recruit Pol η during AID-induced MMR. Only G_1-phase activities of AID or UNG2 are mutagenic in mouse B cells (5, 6, 23). Strong evidence for mutagenic interaction between BER and MMR implies that mutagenic MMR also occurs in G_1 phase (2, 3, 8, 9, 12, 21). dNTP levels were reported to be lowest in G_1 phase, especially in the nucleus (24). We proposed, therefore, that dNTP pools may be inadequate to support long-patch DNA synthesis by conventional DNA polymerases during G_1-phase MMR; polymerase stalling could then induce PCNA ubiquitination (ref. 25; also see ref. 20). The rate-limiting enzyme for dNTP production is ribonucleotide reductase (RNR), which is downregulated in G_1-phase cells via turnover of the R2 subunit (26). However, the major regulator of dNTP levels is not in fact RNR activity, but the deoxynucleotide triphosphohydrolase SAMHD1; dNTPs increase more than 10-fold in resting and proliferating *Samhd1*$^{-/-}$ cells (27, 28). SAMHD1 is a potent restrictor of virus

Significance

Antibody affinity rises during immune responses to viruses via antibody gene somatic hypermutation and Darwinian selection of mutated B cells—in a time frame of days. The enzyme activation-induced deaminase (AID) initiates hypermutation by deaminating genomic cytosines. Mutation is exacerbated by noncanonical G_1-phase DNA repair pathways that deploy error-prone polymerases, including Pol η (gene *Polh*). In G_1 phase, dNTP levels are restricted to inhibit viral replication. We derestricted G_1-phase dNTP supply in hypermutating B cells, which increased virus susceptibility in vitro and caused changes in antibody hypermutation in vivo akin to *Polh* inactivation. We conclude that G_1-phase dNTP paucity contributes to antibody hypermutation and that the evolution of antibody hypermutation included the repurposing of intracellular antivirus mechanisms based on dNTP starvation.

Author contributions: C.J.J. designed research; E.S.T., D.B., T.D., I.S., M.v.G., Z.J., C.S., R.B., and C.J.J. performed research; J.H., W.W., B.K., and R.B. contributed new reagents/analytic tools; E.S.T. and C.J.J. analyzed data; and E.S.T. and C.J.J. wrote the paper.

The authors declare no conflict of interest.

This article is a PNAS Direct Submission. D.G.S. is a guest editor invited by the Editorial Board.

Data deposition: The somatic *Igh V*-region sequences reported in this paper have been deposited in the GenBank database (accession nos. MH198782–MH200576).

[1]To whom correspondence should be addressed. Email: c.jolly@centenary.org.au.

This article contains supporting information online at www.pnas.org/lookup/suppl/doi:10.1073/pnas.1719771115/-/DCSupplemental.

Published online April 18, 2018.

replication (27, 28), and its activity is highest in G_1 phase (29). We quantified *Ig* hypermutation in mouse germinal center B cells lacking SAMHD1. We observed an increase in transitions at C/G and major decreases in transversions at A/T and C/G, which suggests that SAMHD1-induced dNTP paucity contributes to AID-induced mutagenesis via both MMR and uracil BER.

Results

RNR and SAMHD1 Expression in Mouse B Cells. Ribonucleotide reductase (RNR) consists of R1 and R2 subunits, which form a catalytic site at R1/R2 interfaces (reviewed in ref. 30). Consistent with reports for other cell types (30), R2 levels were substantially lower in G_1-phase B cells [i.e., in $mKO2^{+ve}mAG^{-ve}$ (orange) *Fucci*-transgenic B cells; ref. 31] than in the rest of the cell cycle [i.e., in $mKO2^{-ve}mAG^{+ve}$ (green) *Fucci*- transgenic B cells; Fig. 1*A*], implying that B cells carry out far less de novo deoxynucleotide synthesis in G_1 phase than in S phase. SAMHD1 levels were not obviously cell cycle regulated in mouse B cells (Fig. 1*A*), which was consistent with posttranslational modification being the principal regulator of SAMHD1 activity (29).

***Samhd1* Inactivation Substantially Decreased Transversions in *Ig* Genes.** We CRISPR-targeted *Samhd1* exon 1 in C57BL/6 mouse embryos. *Samhd1* alleles carrying 25- or 41-bp frame-shift deletions ("Δ") in exon 1 (Fig. S2) appeared to be knockout alleles (Fig. 1*A*). CRISPR mutation of *Samhd1* enhanced retroviral transduction ($P = 0.0042$; Fig. 1*B*) and substantially increased the levels of dNTPs in resting and blasting B cells ($P < 0.0001$, $P = 0.0003$, respectively) and in G_1-phase cells (Fig. 1*C*). Purines (dATP and dGTP) were increased more than pyrimidines (dTTP and dCTP; Fig. 1*C*). These transduction and dNTP data closely reproduced data generated using conventional $Samhd1^{-/-}$ mice (28, 32, 33).

We four times back-crossed $Samhd1^{\Delta}$ alleles to *Ig*-transgenic "SW_{HEL}" mice, which have a C57BL/6 background, then bred $Samhd1^{\Delta 25/\Delta 25}SW_{HEL}$ mice (and later, $Samhd1^{\Delta 41/\Delta 41}SW_{HEL}$ mice). To quantify *Ig* hypermutation, we ex vivo transduced SW_{HEL} B cells, which are specific for hen egg lysozyme (HEL), to express the PSB2 uracil glycosylase inhibitor and/or GFP then adoptively transferred GFP-positive cells into congenic hosts and immunized with HEL conjugated to SRBC, as outlined in Fig. 2*A* and described previously (6, 9, 25). Adoptive cells are T-dependent and concentrate in germinal centers soon after transfer (25, 34). *Igh* mutations were collated in a 560-bp window from ≤47 single HEL-binding GFP^{+ve} cells per host, sorted from spleens 6 d after adoptive transfer, using a minimum of three donors and hosts per treatment (*Methods*). This procedure results in reproducible hypermutation with minimal impact on the mutation spectrum by antigen selection, because the BCR analyzed starts with high affinity for HEL and the duration of hypermutation (i.e., 6 d) is short (9). Our model predicted that loss of SAMHD1 would decrease mutation at A:T base pairs, and we indeed found this to be the case ($P < 0.0001$ for mutation at A; $P = 0.029$ for mutation at T; Fig. S3*A*). Specifically, *Samhd1* inactivation reduced the frequency of transversion mutations at A:T base pairs (hereon called "A/T transversions"), relative to wild-type cells ($P < 0.0001$; Fig. 2 *B*, *i*), but barely changed the frequency of A/T transitions (Fig. 2 *B*, *ii*). *Samhd1* inactivation also substantially reduced C/G transversions ($P < 0.0001$; Fig. 2 *B*, *iii*) and nearly doubled C/G transitions ($P = 0.0041$; Fig. 2 *B*, *iv*). This increase in C/G transitions partly compensated for the loss of A/T and C/G transversion mutations; total *Ig* mutation in $Samhd1^{\Delta/\Delta}$ B cells was lower than in wild-type cells (Table 1), but not significantly so ($P = 0.07$ by one-way ANOVA). See Table 1 and Figs. S3 and S4 for overviews of the mutation data. *Samhd1* inactivation reduced all classes of C/G transversions. That is C/G to G/C transversions, which are introduced by REV1 via BER and by Pol η via MMR (11, 12, 35), and C/G to A/T transversions, which are introduced by a polymerase or polymerases currently unknown (Table 1 and Fig. S3*A*).

To test whether the impact of *Samhd1* inactivation on *Ig* hypermutation was an artifact of antigen selection, we quantified mutation in intron sequences immediately 3′ to the VDJ_H exon (Fig. S3*B*). Our 560-bp sequence window included the 5′ 101 bp of the J-C_H intron (Fig. S4); this region is analogous to that commonly analyzed in Peyers patch B cells (5, 36)—albeit, with the SW_{HEL} intron carrying a deletion that tags gene-targeted cells (34). *Samhd1* inactivation caused significant reductions in transversions at A/T ($P = 0.0089$) and at C/G ($P = 0.0001$) in the J-C_H intron and increased C/G transitions, albeit not significantly ($P = 0.065$; Fig. S3*B*), relative to wild-type cells. We conclude that the impact of *Samhd1* inactivation on *Ig* hypermutation—in particular, reduced transversion mutation—was not an artifact of antigen selection.

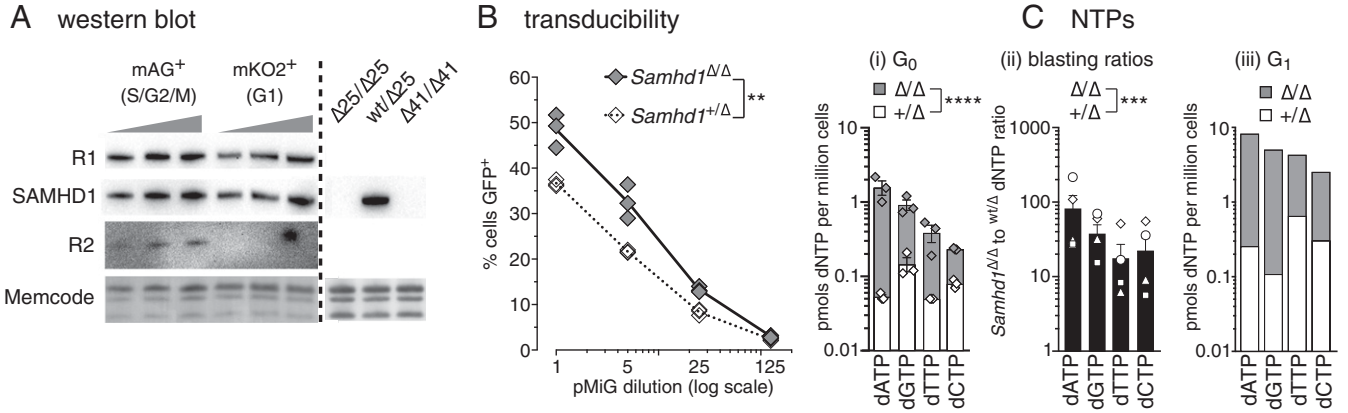

Fig. 1. (*A*) Western blot for RNR subunits (R1 = 90 kDa; R2 = 45 kDa) or SAMHD1 (76 kDa) extracted from splenic B cells after culture for 3 d in LPS. *Fucci*-red/*Fucci*-green transgenic B cells were sorted into green (mAG^+mKO2^-) and orange (mAG^-mKO2^+) populations. Memcode staining (~10- to 20-kDa region) indicates protein loading and transfer. In *Fucci* cells, $mKO2^+$ cells are in G_1 phase and mAG^+ cells are in S, G_2, and M phases (6, 60). (*B*) Transducibility of $Samhd1^{\Delta/\Delta}$ B cells. Splenocytes were cultured with LPS for 1 d to activate B cells, then transduced in triplicates with serially diluted pMiG retrovirus. Frequencies of GFP^+ cells were determined by cytometry 2 d later. $^{**}P = 0.0042$, two-way ANOVA. (*C*) dNTPs measured in whole-cell extracts. (*C*, *i*) dNTPs per 10^6 resting splenocytes, measured in three independent experiments. $^{****}P < 0.0001$, two-way ANOVA. (*C*, *ii* and *iii*) Splenocytes were activated with LPS, and dNTPs were extracted from live cells purified by sedimentation over Histopaque 1083 2 d after activation (*ii*). The ratio of $Samhd1^{\Delta/\Delta}$ dNTPs to $Samhd1^{w.t./\Delta}$ dNTPs is shown for four independent experiments. $^{***}P = 0.0003$, two-way ANOVA. (*C*, *iii*) One day after LPS activation, cells were transduced to express mKO2-cdt fusion protein, which tagged $G_{0/1}$ cells with orange fluorescence (6). Blasting $mKO2^+$ cells were purified by flow cytometry 2 d later.

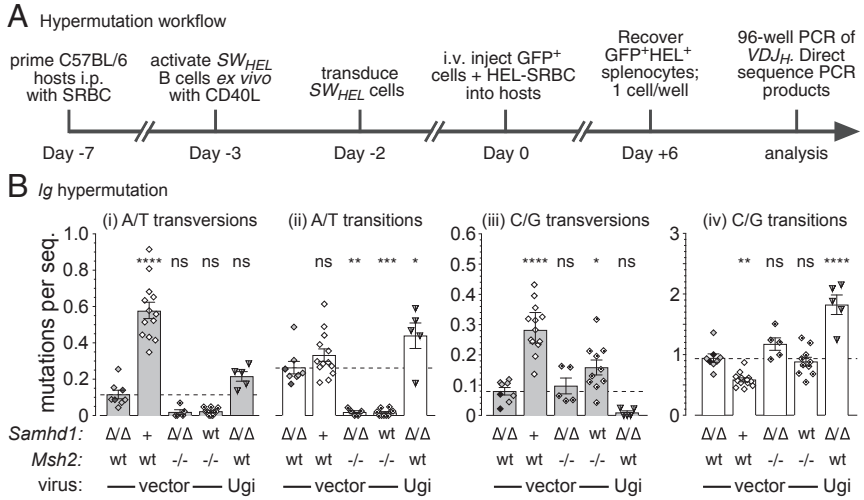

Fig. 2. *Igh* hypermutation in transduced germinal center B cells. (*A*) Experiment design. (*B*) Each symbol represents the mean *Igh* mutations (in a 560-bp sequence window) for ~45 transduced cells sorted from one host mouse. Histograms represent the means (±SEM) of hosts. Mutations are divided into transversions at A:T (*i*), transitions at A:T (*ii*), transversions at C:G (*iii*), and transitions at C:G (*iv*). Symbols: white, $Samhd1^{wt}$ (thin border) or $Samhd1^{+/\Delta 25}$ (bold border); gray, $Samhd1^{\Delta 25/\Delta 25}$; black; $Samhd1^{\Delta 41/\Delta 41}$; black dot, $Msh2^{-/-}$. Transduced with: diamonds, pMiG; triangles, pM/ugi-GFP. Significant differences (one-way ANOVA with Holm-Sidak's post hoc tests) to the vector-transduced $Samhd1^{\Delta 25/\Delta 25}$ means (i.e., the dashed line) are indicated: $^*P < 0.05$; $^{**}P < 0.01$; $^{***}P < 0.001$; $^{****}P < 0.0001$; ns, not significant.

***Samhd1* Inactivation Does Not Phenocopy MMR Inhibition.** Like *Samhd1* inactivation, *Msh2* knockout decreases A/T mutations and C/G transversions in SW_{HEL} B cells (9) (Fig. 2, Table 1, and Fig. S3). This raised the possibility that *Samhd1* inactivation acted by partially inhibiting AID-induced MMR. A hallmark feature of MMR knockout is the focusing of AID-induced mutation on hotspot motifs, especially AGCW motifs (see ref. 9 and Table S1). We therefore examined our mutation data for hotspot focusing (Fig. 3) and measured hypermutation in adoptive $Msh2^{-/-}Samhd1^{\Delta 25/\Delta 25}$ SW_{HEL} B cells (Figs. 2*B* and 3, Table 1, and Figs. S3 and S4). In summary, we found that *Samhd1* inactivation did not focus AID-induced mutation on AGCW hotspots, an outcome quite different to loss of MMR (see overviews in Table S1).

The strand bias of mutation changes further distinguished $Samhd1^{\Delta/\Delta}$ from $Msh2^{-/-}$ cells. As described before (e.g., ref. 9), $Msh2^{-/-}$ altered mutations at C nearly twice as much as at G. In contrast, *Samhd1* inactivation altered mutation at C and at G to comparable extents (Fig. S3*A*).

***Samhd1* Inactivation Does Not Inhibit Uracil Repair via UNG2.** Reduced C/G transversion in $Samhd1^{\Delta/\Delta}$ B cells raised the obvious possibility that uracil excision by UNG2 might partially depend on SAMHD1, via some unexpected mechanism. To measure UNG2-mediated uracil repair, we blockaded UNG2 activity in adoptive $Samhd1^{\Delta/\Delta}$ cells using retroviral expression of the uracil glycosylase inhibitor (ugi) from bacteriophage PSB2 (37). Previous blockades of UNG activity in wild-type SW_{HEL} B cells with ugi increased *Igh* C/G transitions 2.3-fold, in a strand-unbiased manner, presumably by increasing "ignorant" replication opposite persistent uracils (6, 9). In $Samhd1^{\Delta/\Delta}$ B cells, retroviral expression of ugi-GFP increased C/G transitions by 1.9-fold ($P < 0.0001$), relative to expression of GFP alone (Fig. 2 *B*, *iv*), and this increase was strand-unbiased (Table 1 and Fig. S3*A*). This demonstrated that UNG2 mediates reversion of similar frequencies of U:G base pairs into C:G base pairs in hypermutating *Igh* genes regardless of SAMHD1 activity, so it is unlikely SAMHD1 alters uracil excision rates by UNG2.

Discussion

***Samhd1* Inactivation Partially Phenocopies Genotypes That Block Pol η Recruitment.** We, and later others, proposed polymerase stalling induced by dNTP imbalances as a G_1-phase mechanism that could explain PCNA ubiquitination, Pol η recruitment, and nucleotide misincorporation during AID-induced MMR (20, 25). Our finding here of reduced A/T mutation in $Samhd1^{\Delta/\Delta}$ cells (Fig. S3*A*) was predicted by this model but does not prove it. The unequal impact of *Samhd1* inactivation on A/T transversions versus A/T transitions (Fig. 2*B* and Fig. S3*B*) was not expected but might be explained by the greater impact of *Samhd1* inactivation on purine dNTPs over pyrimidine dNTPs (see below and Fig. 4). *Samhd1*-CRISPR also decreased C/G transversions

Table 1. Raw mutation data

						No. of mutations											
						From G (124 bases) to:			From C (131 bases) to:			From A (135 bases) to:			From T (170 bases) to:			TOTAL
Cells	Protein	No. of Hosts	No. of Sequences	No. of Deletions*	No. of Insertions*	A	C	T	T	G	A	G	T	C	C	A	G	Per sequence
WT or $Samhd1^{+/\Delta}$	GFP	13	565	9,2,1	0	190	74	35	142	26	27	125	170	87	64	44	28	1.79
$Samhd1^{\Delta/\Delta}$	GFP	8	354	1	1	191	12	4	144	10	2	60	15	7	32	11	8	1.40
$Msh2^{-/-}Samhd1^{\Delta/\Delta}$	GFP	5	213	1,2,15,5,1	0	129	11	3	122	2	5	3	1	2	1	1	0	1.31
$Msh2^{-/-}$	GFP	10	446	10,3	0	183	40	18	210	5	7	5	5	3	2	2	0	1.08
$Samhd1^{\Delta/\Delta}$	ugi-GFP	5	218	0	0	235	0	1	163	0	1	61	20	12	34	6	8	2.48

*The size (bp) of all deletions or insertions observed is listed, separated by commas.

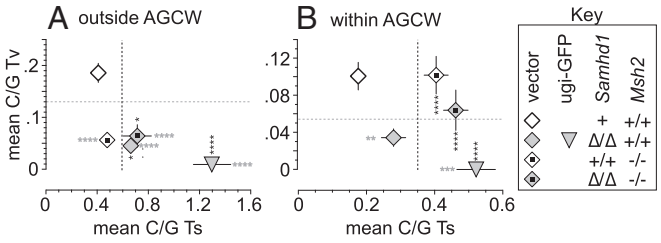

Fig. 3. Occurrence of C/G transitions (*x* axes) or transversions (*y* axes) outside or within AGCW motifs. The mean (±SEM) number of C/G transitions or transversions per 560-bp sequence were calculated on a per host basis, as in Fig. 2, for C/G located outside AGCW motifs (*A*) or C/G located inside AGCW motifs (*B*). Significant differences to the vector-transduced *Samhd1*$^{+}$ means are indicated with asterisks (one-way ANOVA, Holm–Sidak's post hoc tests): vertical and black for C/G transitions; horizontal and gray for C/G transversions. All means lying to the right of the vertical dotted line represent significantly elevated C/G transition frequencies, and all means lying below the gray dotted line represent significantly reduced C/G transversion frequencies, relative to the *Samhd1*$^{+}$*Msh2*$^{+/+}$ data.

and increased C/G transitions in a strand unbiased manner that was not focused on AGCW hotspots (Figs. 2 and 3, Figs. S3 and S4, and Table S1). We largely ruled out reduced uracil excision via MMR or UNG2 as the cause of this. Reduced A/T mutations decoupled from an increase in focus on AGCW hotspots was observed previously in *Polh*$^{-/-}$ and *Pcna*$^{K164R/K164R}$ mice (21, 38), and contrasts with MMR deficiency, which couples these two mutation characteristics, regardless of *Samhd1, Pcna*, or *Polh* genotype (Fig. 3; see also phenotypes summarized in Table S1). The contrast in hotspot focusing among *Samhd1*$^{\Delta/\Delta}$, *Polh*$^{-/-}$, and *Pcna*$^{K164R/K164R}$ on the one hand, and *Msh2*$^{-/-}$, *Msh6*$^{-/-}$, and *Exo1*$^{-/-}$ on the other, can be explained by the likelihood that the former genetic manipulations do not prevent mismatch excision and only impact excision patch in-fill, while the latter manipulations prevent both. We interpret the similarities in the hypermutation phenotypes of *Polh*$^{-/-}$, *Pcna*$^{K164R/K164}$, and *Samhd1*$^{\Delta/\Delta}$ B cells as consistent with *Samhd1* inactivation reducing PCNA ubiquitination and Pol η recruitment during AID-induced MMR, without reducing the production of mismatch excision patches. Nonetheless, our data do not prove this model. Differences in the precise frequencies of mutation subclasses in *Polh*$^{-/-}$, *Pcna*$^{K164R/K164}$, and *Samhd1*$^{\Delta/\Delta}$ B cells (summarized in Table S1) might be ascribed to differences in the polymerases recruited downstream of AID, as well as the unique dNTP milieu in *Samhd1*$^{\Delta/\Delta}$ cells. For instance, Pol δ and Pol κ are likely to be recruited to in-fill MMR excision patches in *PCNA*$^{K164R/K164R}$ and *Polh*$^{-/-}$ B cells, respectively (18).

Unlike the *Msh2*$^{-/-}$, *PCNA*$^{K164R/K164R}$, and *Polh*$^{-/-}$ mutations, *Samhd1* inactivation did not suppress A/T transitions, although it suppressed A/T transversions (Fig. 2*B* and Fig. S3*B*). This may reflect the fact that *Samhd1* inactivation skewed the dNTP pool toward purines (Fig. 1*C*), which would increase bias toward incorporation of dA and dG, regardless of the polymerase used. Since mismatch excision downstream of AID is heavily skewed to the top strand (5, 9), this would result in bias toward incorporation of dA and dG opposite bottom-strand dT during AID-induced MMR (Fig. 4). Thus, the A/T mutation phenotype of *Samhd1*$^{\Delta/\Delta}$ B cells can theoretically be explained by altered polymerase recruitment, as a consequence of better dNTP supply, combined with bias toward top-strand purine incorporation during MMR. Would A/T mutation disappear altogether in a hypothetical situation where G_1-phase dNTP pools perfectly mimicked S phase? We doubt it: The corequirement for UNG2 and MMR for almost half of *Ig* C/G transversions implies that UNG2-derived AP sites are encountered by polymerases during AID-induced MMR (9, 39, 40). This could induce a baseline of polymerase stalling and PCNA ubiquitination regardless of dNTP supply. The role of Ub-PCNA in AID-induced MMR might therefore be explained by a combination of both polymerase encounter with AP sites and SAMHD1-induced dNTP paucity.

The hypermutation phenotypes of *Ung*$^{-/-}$, *Rev1*$^{-/-}$, and *Polb*$^{-/-}$ B cells suggest that most C/G transversions are created by translesion bypass of AP sites, with a minority (~15%) created by simple misincorporation at C/G during MMR, long-patch BER, or single-nucleotide BER (10, 13, 35). We speculate that the substantially reduced C/G transversion and increased C/G transition mutation in *Samhd1*$^{\Delta/\Delta}$ cells is again most simply explained by bias toward purine misincorporation over pyrimidine misincorporation—this time during UNG2-induced lesion bypass events, as illustrated in Fig. 4. It is possible that SAMHD1's exonuclease activity and/or its capacity to recruit the endonuclease CtIP (41, 42) influences *Ig* mutation, rather than its dNTPase activity. The production of double-strand breaks (DSB) downstream of AID is critical for *Ig* class switching (1), but DSB formation plays a minor role in V-region hypermutation (43–45). In our experiments, insertions and deletions, which likely arise from DSB, were not discernably affected by *Samhd1* inactivation (Table 1) and clustered near AGCW motifs regardless of *Samhd1* genotype (Fig. S4).

An Entirely G_1-Phase Model of *Ig* Hypermutation. We suggested previously that MMR-independent lesion bypass might occur when G_1-phase AP sites persist into S phase and are replicated (6; see Fig. S1). This model is not explicitly contradicted by the *Samhd1*$^{\Delta/\Delta}$ phenotype we report here, because *Samhd1* inactivation produced supraoptimal dNTPs in all cell cycle phases. However, we recently identified an ~20-bp footprint flanking AGCW sites within which C/G transversions occurred independently of MMR (9). In remarkable convergence with this footprint size, Woodrick et al. (46) showed that LP-BER produces excision patches centered on the excised AP site that are ≤20 nucleotides long; they further showed that LP-BER predominates over single-nucleotide BER in living cells. AGCW motifs are the only hotspots where AID can deaminate either DNA strand with comparable efficiency in vivo (8, 9, 47). This leads us to update the *Ig* hypermutation model and propose that MMR-independent C/G transversions occur via simultaneous G_1-phase LP-BER of deaminations that have accumulated in

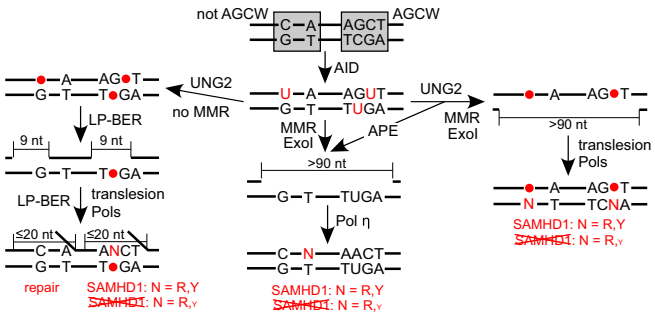

Fig. 4. A completely G_1-phase model of *Ig* hypermutation that incorporates SAMHD1 and a major role for LP-BER. If both strands of an AGCW motif are deaminated, then LP-BER in one strand can expose an AP site in the other, whereas single-nucleotide BER cannot. At deamination sites >10 bases away from AGCW motifs, the chance that excision during LP-BER will expose another AP site in the opposite strand is much lower. Recruitment of ExoI via MutSα produces much longer excision patches (>90 bases long; ref. 61) than LP-BER's 20-base excision patch (46). In UNG2^{+} cells, these long excision patches have a roughly equal chance of exposing an AP site in the opposite strand regardless of where the deamination site that recruited MutSα lies. SAMHD1 activity determines the dNTP milieu, thus dictating the misincorporation spectrum for both MMR and LP-BER. This model explains (*i*) the hyperfocusing of *Ig* mutation on AGCW motifs that occurs only in UNG2^{+} MMR-deficient B cells and not in UNG2/MMR double-deficient cells (9, 21), (*ii*) the near complete MMR dependence of C/G transversion mutation at sites >10 bases from AGCW motifs (9), (*iii*) increased C/G transitions, and (*iv*) substantially decreased A/T and C/G transversions in *Samhd1*$^{\Delta/\Delta}$ B cells (this work).

opposite strands of AGCW sites, as illustrated in Fig. 4, without any requirement for AP sites to persist into S phase. A key strength of this model is its ability to explain why UNG2 is at its most error-prone in regions where AGCW motifs are concentrated.

Similarities Between *Ig* Hypermutation and Intracellular Virus Restriction Mechanisms. Cell cycle turnover of RNR and the dNTPase activity of SAMHD1 are intracellular antiviral mechanisms that evolved long before the appearance of adaptive immunity (48). The APOBEC3 family of AID paralogues also restrict viral infection by deaminating viral genomes; UNG2 and APE activities downstream of APOBEC3 can contribute to viral restriction (49, 50). AID/APOBEC-like deaminases occur across metazoa, dictyosteliida, and even algae, and may have evolved in an arms race with viruses and retro elements (51). Here, we've shown that SAMHD1 is another virus restriction factor that contributes to the mutagenicity of AID—by promoting transversion mutation downstream of AID. Transition mutation is the most common form of point mutation in the genome. Codon degeneracy has evolved to accommodate this, which means that transversion mutations are generally more mutagenic than transition mutations (52), implying that *Ig* point mutations likely to cause the greatest changes in antibody binding characteristics are promoted by SAMHD1. For example, the generation of high-affinity anti-phenyloxazalone antibodies in BALB/c mice predominantly involves H34N and Y36F mutation of $V_\kappa Ox1/J_\kappa 5$ rearrangements: a C to A transversion and an A to T transversion, respectively (53). It's conceivable that G_1-phase MMR can also act as an antiviral mechanism, because repeated recruitment of ExoI to viral genomes that misincorporated G_1-phase dNTPs would inhibit viral replication. Given that G_1-phase nicking by MutLα in B cells does not discriminate between mutated and nonmutated DNA strands (5), it is further conceivable that G_1-phase MMR evolved to attack viral genomes and trigger apoptosis, rather than to repair errors, and was then coopted by *Ig* hypermutation, along with UNG2 and SAMHD1, as part of a preexisting suite of ancient intracellular antivirus mechanisms.

Materials and Methods

Mice. Male C57BL/6 host mice were initially purchased from Animal Resources Centre (Canning Vale, Western Australia) and later from Australian BioResources (Moss Vale, New South Wales), and were used in experiments when 8–16 wk old. *Msh2*^{ko}, *Rag1*^{ko}, *Igh*-knock-in/*Igk*-transgenic SW_{HEL}, and *Fucci*-red/*Fucci*-green mice (25, 31, 34, 54) were interbred and maintained on a C57BL/6 background under SPF conditions in the Centenary Institute Animal Facility.

Samhd1$^{\Delta/\Delta}$ mice were produced by the Mouse Engineering Garvan/ABR (MEGA) Facility (Moss Vale and Sydney, Australia) by CRISPR/Cas9 gene targeting in C57BL/6J mouse embryos following established molecular and animal husbandry techniques (55). To minimize off-target genome modifications, the double-nicking approach employing the single-strand cleaving mutant of the Cas9 endonuclease (Asp10Ala = Cas9n) was employed (56). For this purpose, paired single-guide RNAs (sgRNAs) were designed to target within the first coding exon (Exon 1) of *Samhd1*. The sites used were CTCCAAGGGTGCGCTCTGCATGG and GCTAAGCGACCCCGCTGCGATGG (protospacer-associated motifs = PAMs underlined).

To target *Samhd1*, a solution consisting of the two sgRNAs (15 ng/μL each) and full-length, polyadenylated Cas9n mRNA (30 ng/μL) was prepared and microinjected into the nucleus and cytoplasm of SW_{HEL} × C57BL/6 zygotes. Microinjected embryos were cultured overnight and introduced into pseudopregnant foster mothers. Pups were screened by PCR across the two target sites and Sanger sequencing to detect those with modifications to *Samhd1*. Independent founders carrying 25- and 41-bp frame-shift deletions within Exon 1 were selected, backcrossed to wild-type SW_{HEL} (C57BL/6J) mice four times, and the progeny was intercrossed to derive homozygous *Samhd1*$^{\Delta 25/\Delta 25}$ and *Samhd1*$^{\Delta 41/\Delta 41}$ lines.

All work was carried out with approval from and oversight by the Royal Prince Alfred Hospital Animal Welfare and Biosafety Committees, in accordance with NSW and Federal Australian legislation and the *Australian Code for the Care and Use of Animals for Scientific Purposes* (57).

Plasmids and Retroviruses. pMiG-based retroviruses expressing mKO2-cdt fusion protein (whose accumulation is restricted to G_0/G_1-phases by the degron from human Cdt1), EGFP, or ugi-EGFP fusion protein have been described (6). All cDNAs were cloned into the pMiG vector (58) using conventional techniques and verified by Sanger sequencing (Macrogen Inc). Ecotropic viral supernatants were produced by calcium phosphate transfection of the Platinum-E retroviral packaging cell line (Cell Biolabs, Inc.) as described (9). Culture medium (DMEM, 10% bovine calf serum, 1 mM sodium pyruvate, 2 mM L-alanyl-L-glutamine dipeptide, penicillin/streptomycin) was replaced at 12 h, then retroviral supernatants were harvested at 60 h, 0.45-μm filtered, snap frozen in liquid nitrogen, and stored at −70 °C.

Transduction and Adoptive Transfer of SW_{HEL} Splenocytes and Mutation Analysis. Activation of mouse splenocytes with recombinant CD40L for 24 h, followed by transduction in culture for a further 48 h has been described (9). GFP$^+$ cells were sorted using a BD FACS Aria II or BD influx sorter, mixed with sheep red blood cells (SRBC; Applied Biological Products Management) conjugated to hen egg lysozyme (HEL; Sigma-Aldrich) in B cell medium (54) and injected into host tail veins as a bolus of $\leq 10^4$ HEL-binding B cells plus 10^8 HEL-SRBC into 8- to 12-wk-old male hosts that had been primed i.p. 7 d prior with 10^8 SRBC in PBS, as described (34). Six days after adoptive transfer, host spleens were harvested, depleted of RBC using Histopaque 1083 fractionation (Sigma-Aldrich), and GFP$^+$ HEL-binding cells were sorted using a BD FACS Aria II or BD influx, one cell per well into 96-well PCR plates (4titude) containing 15 μL per well of ice-cold Mg-free 1× Taq DNA polymerase buffer (Promega "Go-Taq" buffer) supplemented to include 0.1 mM EDTA, 1% Tween-20 detergent (Astral Scientific) and 0.25 mg/mL proteinase K (Roche Diagnostics). Single-cell nested PCR of the singular gene-targeted SW_{HEL} VDJ_H rearrangement present in each cell was performed as described (25). Single allele mutation data were collected from up to 47 single cells using direct Sanger sequencing (Macrogen) of single-cell PCR products, as described (25), except that the sequencing primer (jol27: 5′-ACTC CACC AACA CCAT CACA C-3′) was positioned further 3′ to the start codon than previously, enlarging the sequence window from 523 bases to 560 bases. Each treatment involved at least three individual donors and hosts. Mutation data were analyzed by one-way ANOVA and Holm–Sidak's post hoc multiple comparisons tests with Prism 7 for MacOS (GraphPad Software, Inc), using the mean mutation of each hosts' sampled cells as a single data point (9).

Western Blot Analysis. B cells from *Fucci*-red/*Fucci*-green double-transgenic mice (31) were cultured in 20 μg/mL *S. typhosa* LPS (Sigma-Aldrich) plus 20 ng/mL mouse IL-4 (BD Biosciences) for 3 d to induce robust B cell proliferation. B cells from *Fucci* mice express an orange fluorescent fusion protein ("mKO2-cdt") in G_1 phase of the cell cycle or a green fluorescent fusion protein ("mAG-gmnn") in S, G_2, and M phases (31). Transduced cells were sorted into mKO2$^+$mAG$^-$ (G_1 phase) and mKO2$^-$mAG$^+$ ($S/G_2/M$ phase) fractions using a BD Influx sorter. Proteins were extracted from cells by vortexing cell pellets at 2×10^7 cells per mL in Laemmli sample buffer (0.1% 2-mercaptoethanol, 2% SDS, 10% glycerol, 0.0005% bromophenol blue, 63 mM Tris·Cl, pH 6.8), then incubating for 30 min at 20 °C with 250 units/mL Benzonase nuclease (Millipore). Extracts were electrophoresed using 4–12% Bolt Bis-Tris Plus polyacrylamide gels (Invitrogen) and transferred to nitrocellulose membranes using a Novex semi-dry blotter (Invitrogen) according to manufacturer protocols. Membranes were blocked for 1 h with 5% (wt/vol) skim milk powder in TBST [0.9% (wt/vol) NaCl, 0.1% (vol/vol) Tween-20 and 10 mM Tris·HCl, pH 7.4] at room temperature, then incubated overnight at 4 °C with mouse anti-SAMHD1 IgG2b monoclonal OTI1A1 (Abcam), goat anti-R2 IgG polyconal E-16 (Santa Cruz Biotechnology), or rabbit anti-R1 IgG monoclonal EPR8483 (Abcam) in skim milk/TBST. Washed membranes were incubated with species-appropriate secondary antibodies conjugated to horseradish peroxidase (Santa Cruz Biotechnology) for 1 h at 20 °C in skim milk/TBST, then washed again and incubated with SuperSignal West Pico Chemiluminescent Substrate (Thermo Fisher). Luminescence was recorded using a ChemiDoc MP (Bio-Rad).

dNTP Quantitation. *Samhd1*$^{\Delta 25/\Delta 25}$ or *Samhd1*$^{+/\Delta 25}$ splenocytes were cultured with LPS plus IL-4, for 24 h as above. Activated cells were then transduced with fresh retroviral supernatants of pMiG-derived retroviruses that expressed mKO2-cdt; cells expressing mKO2-cdt fluoresce red when they are in G_1 phase (6, 31). Two days later, orange-fluorescent (i.e., G_1-phase) cells were sorted using a BD Influx sorter into ice-cold bovine serum. Total dNTPs were extracted from PBS-washed sorted cells using ice-cold 60% aqueous methanol, as described (59). Resting or nonfractionated proliferating *Samhd1*$^{\Delta 25/\Delta 25}$ or *Samhd1*$^{+/\Delta 25}$ splenocytes depleted of RBC and dead cells using density gradient centrifugation over Histopaque 1083 (Sigma-Aldrich) were also extracted. dNTPs were then quantified using an HIV reverse transcriptase primer extension assay, as described (59).

ACKNOWLEDGMENTS. We thank Sydney Cytometry (Centenary Institute/The University of Sydney) for the provision of cell sorting facilities and expertise, and Australian BioResources and the Centenary Institute Animal Facility for the provision of mouse care and breeding. This research was supported by National Health and Medical Research Council Project Grants 1067891 and 1051820 (to C.J.J.), an Australian Postgraduate Award (to E.S.T.), NIH Grants AI049781 and GM104198 (to B.K.), and a Centenary Foundation grant (to C.J.J.).

1. Methot SP, Di Noia JM (2017) Molecular mechanisms of somatic hypermutation and class switch recombination. *Adv Immunol* 133:37–87.
2. Rada C, Di Noia JM, Neuberger MS (2004) Mismatch recognition and uracil excision provide complementary paths to both Ig switching and the A/T-focused phase of somatic mutation. *Mol Cell* 16:163–171.
3. Shen HM, Tanaka A, Bozek G, Nicolae D, Storb U (2006) Somatic hypermutation and class switch recombination in Msh6(-/-)Ung(-/-) double-knockout mice. *J Immunol* 177: 5386–5392.
4. Dingler FA, Kemmerich K, Neuberger MS, Rada C (2014) Uracil excision by endogenous SMUG1 glycosylase promotes efficient Ig class switching and impacts on A:T substitutions during somatic mutation. *Eur J Immunol* 44:1925–1935.
5. Girelli Zubani G, et al. (2017) Pms2 and uracil-DNA glycosylases act jointly in the mismatch repair pathway to generate Ig gene mutations at A-T base pairs. *J Exp Med* 214:1169–1180.
6. Sharbeen G, Yee CW, Smith AL, Jolly CJ (2012) Ectopic restriction of DNA repair reveals that UNG2 excises AID-induced uracils predominantly or exclusively during G1 phase. *J Exp Med* 209:965–974.
7. Pérez-Durán P, et al. (2012) UNG shapes the specificity of AID-induced somatic hypermutation. *J Exp Med* 209:1379–1389.
8. Chen Z, et al. (2016) Interplay between target sequences and repair pathways determines distinct outcomes of AID-initiated lesions. *J Immunol* 196:2335–2347.
9. Thientosapol ES, et al. (2017) Proximity to AGCT sequences dictates MMR-independent versus MMR-dependent mechanisms for AID-induced mutation via UNG2. *Nucleic Acids Res* 45:3146–3157.
10. Esposito G, et al. (2000) Mice reconstituted with DNA polymerase beta-deficient fetal liver cells are able to mount a T cell-dependent immune response and mutate their Ig genes normally. *Proc Natl Acad Sci USA* 97:1166–1171.
11. Kano C, Hanaoka F, Wang JY (2012) Analysis of mice deficient in both REV1 catalytic activity and POLH reveals an unexpected role for POLH in the generation of C to G and G to C transversions during Ig gene hypermutation. *Int Immunol* 24:169–174.
12. Krijger PH, et al. (2013) Rev1 is essential in generating G to C transversions downstream of the Ung2 pathway but not the Msh2+Ung2 hybrid pathway. *Eur J Immunol* 43:2765–2770.
13. Weill J-C, Reynaud C-A (2008) DNA polymerases in adaptive immunity. *Nat Rev Immunol* 8:302–312.
14. Rada C, Ehrenstein MR, Neuberger MS, Milstein C (1998) Hot spot focusing of somatic hypermutation in MSH2-deficient mice suggests two stages of mutational targeting. *Immunity* 9:135–141.
15. Frey S, et al. (1998) Mismatch repair deficiency interferes with the accumulation of mutations in chronically stimulated B cells and not with the hypermutation process. *Immunity* 9:127–134.
16. Zeng X, et al. (2001) DNA polymerase eta is an A-T mutator in somatic hypermutation of immunoglobulin variable genes. *Nat Immunol* 2:537–541.
17. Bardwell PD, et al. (2004) Altered somatic hypermutation and reduced class-switch recombination in exonuclease 1-mutant mice. *Nat Immunol* 5:224–229.
18. Delbos F, et al. (2005) Contribution of DNA polymerase eta to immunoglobulin gene hypermutation in the mouse. *J Exp Med* 201:1191–1196.
19. Langerak P, Nygren AO, Krijger PH, van den Berk PC, Jacobs H (2007) A/T mutagenesis in hypermutated immunoglobulin genes strongly depends on PCNAK164 modification. *J Exp Med* 204:1989–1998.
20. Peña-Diaz J, et al. (2012) Noncanonical mismatch repair as a source of genomic instability in human cells. *Mol Cell* 47:669–680.
21. Delbos F, Aoufouchi S, Faili A, Weill JC, Reynaud CA (2007) DNA polymerase eta is the sole contributor of A/T modifications during immunoglobulin gene hypermutation in the mouse. *J Exp Med* 204:17–23.
22. Stavnezer J, et al. (2014) Differential expression of APE1 and APE2 in germinal centers promotes error-prone repair and A:T mutations during somatic hypermutation. *Proc Natl Acad Sci USA* 111:9217–9222.
23. Wang Q, et al. (2017) The cell cycle restricts activation-induced cytidine deaminase activity to early G1. *J Exp Med* 214:49–58.
24. Skoog L, Bjursell G (1974) Nuclear and cytoplasmic pools of deoxyribonucleoside triphosphates in Chinese hamster ovary cells. *J Biol Chem* 249:6434–6438.
25. Sharbeen G, et al. (2010) Incorporation of dUTP does not mediate mutation of A:T base pairs in Ig genes in vivo. *Nucleic Acids Res* 38:8120–8130.
26. Rampazzo C, et al. (2010) Regulation by degradation, a cellular defense against deoxyribonucleotide pool imbalances. *Mutat Res* 703:2–10.
27. Franzolin E, et al. (2013) The deoxynucleotide triphosphohydrolase SAMHD1 is a major regulator of DNA precursor pools in mammalian cells. *Proc Natl Acad Sci USA* 110:14272–14277.
28. Behrendt R, et al. (2013) Mouse SAMHD1 has antiretroviral activity and suppresses a spontaneous cell-intrinsic antiviral response. *Cell Rep* 4:689–696.
29. Ballana E, Este JA (2015) SAMHD1: At the crossroads of cell proliferation, immune responses, and virus restriction. *Trends Microbiol* 23:680–692.
30. Nordlund P, Reichard P (2006) Ribonucleotide reductases. *Annu Rev Biochem* 75: 681–706.
31. Aiba Y, et al. (2010) Preferential localization of IgG memory B cells adjacent to contracted germinal centers. *Proc Natl Acad Sci USA* 107:12192–12197.
32. Lahouassa H, et al. (2012) SAMHD1 restricts the replication of human immunodeficiency virus type 1 by depleting the intracellular pool of deoxynucleoside triphosphates. *Nat Immunol* 13:223–228.
33. Rehwinkel J, et al. (2013) SAMHD1-dependent retroviral control and escape in mice. *EMBO J* 32:2454–2462.
34. Phan TG, et al. (2003) B cell receptor-independent stimuli trigger immunoglobulin (Ig) class switch recombination and production of IgG autoantibodies by anergic self-reactive B cells. *J Exp Med* 197:845–860.
35. Jansen JG, et al. (2006) Strand-biased defect in C/G transversions in hypermutating immunoglobulin genes in Rev1-deficient mice. *J Exp Med* 203:319–323.
36. Jolly CJ, Klix N, Neuberger MS (1997) Rapid methods for the analysis of immunoglobulin gene hypermutation: Application to transgenic and gene targeted mice. *Nucleic Acids Res* 25:1913–1919.
37. Mol CD, et al. (1995) Crystal structure of human uracil-DNA glycosylase in complex with a protein inhibitor: Protein mimicry of DNA. *Cell* 82:701–708.
38. Krijger PH, Langerak P, van den Berk PC, Jacobs H (2009) Dependence of nucleotide substitutions on Ung2, Msh2, and PCNA-Ub during somatic hypermutation. *J Exp Med* 206:2603–2611.
39. Schanz S, Castor D, Fischer F, Jiricny J (2009) Interference of mismatch and base excision repair during the processing of adjacent U/G mispairs may play a key role in somatic hypermutation. *Proc Natl Acad Sci USA* 106:5593–5598.
40. Frieder D, Larijani M, Collins C, Shulman M, Martin A (2009) The concerted action of Msh2 and UNG stimulates somatic hypermutation at A. T base pairs. *Mol Cell Biol* 29: 5148–5157.
41. Ryoo J, et al. (2014) The ribonuclease activity of SAMHD1 is required for HIV-1 restriction. *Nat Med* 20:936–941.
42. Daddacha W, et al. (2017) SAMHD1 promotes DNA end resection to facilitate DNA repair by homologous recombination. *Cell Rep* 20:1921–1935.
43. Sale JE, Neuberger MS (1998) TdT-accessible breaks are scattered over the immunoglobulin V domain in a constitutively hypermutating B cell line. *Immunity* 9:859–869.
44. Cook AJ, et al. (2007) DNA-dependent protein kinase inhibits AID-induced antibody gene conversion. *PLoS Biol* 5:e80.
45. Kepler TB, et al. (2014) Immunoglobulin gene insertions and deletions in the affinity maturation of HIV-1 broadly reactive neutralizing antibodies. *Cell Host Microbe* 16: 304–313.
46. Woodrick J, et al. (2017) A new sub-pathway of long-patch base excision repair involving 5′ gap formation. *EMBO J* 36:1605–1622.
47. Xue K, Rada C, Neuberger MS (2006) The in vivo pattern of AID targeting to immunoglobulin switch regions deduced from mutation spectra in msh2-/- ung-/- mice. *J Exp Med* 203:2085–2094.
48. Ayinde D, Casartelli N, Schwartz O (2012) Restricting HIV the SAMHD1 way: Through nucleotide starvation. *Nat Rev Microbiol* 10:675–680.
49. Conticello SG, Thomas CJ, Petersen-Mahrt SK, Neuberger MS (2005) Evolution of the AID/APOBEC family of polynucleotide (deoxy)cytidine deaminases. *Mol Biol Evol* 22: 367–377.
50. Harris RS, Dudley JP (2015) APOBECs and virus restriction. *Virology* 479–480:131–145.
51. Krishnan A, Iyer LM, Holland SJ, Boehm T, Aravind L (2018) Diversification of AID/APOBEC-like deaminases in metazoa: Multiplicity of clades and widespread roles in immunity. *Proc Natl Acad Sci USA* 115:E3201–E3210.
52. Watson JD, et al. (2013) *Molecular Biology of the Gene* (Pearson, Boston), 7th Ed.
53. Griffiths GM, Berek C, Kaartinen M, Milstein C (1984) Somatic mutation and the maturation of immune response to 2-phenyl oxazolone. *Nature* 312:271–275.
54. Cook AJL, et al. (2003) Reduced switching in SCID B cells is associated with altered somatic mutation of recombined S regions. *J Immunol* 171:6556–6564.
55. Yang H, Wang H, Jaenisch R (2014) Generating genetically modified mice using CRISPR/Cas-mediated genome engineering. *Nat Protoc* 9:1956–1968.
56. Ran FA, et al. (2013) Double nicking by RNA-guided CRISPR Cas9 for enhanced genome editing specificity. *Cell* 154:1380–1389.
57. National Health and Medical Research Council (2013) *Australian Code for the Care and Use of Animals for Scientific Purposes* (National Health and Medical Research Council, Canberra, Australia), 8th Ed.
58. Refaeli Y, Van Parijs L, Alexander SI, Abbas AK (2002) Interferon gamma is required for activation-induced death of T lymphocytes. *J Exp Med* 196:999–1005.
59. Diamond TL, et al. (2004) Macrophage tropism of HIV-1 depends on efficient cellular dNTP utilization by reverse transcriptase. *J Biol Chem* 279:51545–51553.
60. Sakaue-Sawano A, et al. (2008) Visualizing spatiotemporal dynamics of multicellular cell-cycle progression. *Cell* 132:487–498.
61. Zivojnovic M, et al. (2014) Somatic hypermutation at A/T-rich oligonucleotide substrates shows different strand polarities in Ung-deficient or -proficient backgrounds. *Mol Cell Biol* 34:2176–2187.